

Clouds in Arms

Vasily A. Belokurov^{1,2*} & Denis Erkal³

¹*Institute of Astronomy, Madingley Rd, Cambridge, CB3 0HA*

²*Center for Computational Astrophysics, Flatiron Institute, 162 5th Avenue, New York, NY 10010, USA*

³*Department of Physics, University of Surrey, Guildford GU2 7XH, UK*

3 August 2018

ABSTRACT

We use astrometry and broad-band photometry from Data Release 2 of the ESA’s Gaia mission to map out low surface-brightness features in the stellar density distribution around the Large and Small Magellanic Clouds. The LMC appears to have grown two thin and long stellar streams in its Northern and Southern regions, highly reminiscent of spiral arms. We use computer simulations of the Magellanic Clouds’ in-fall to demonstrate that these arms were likely pulled out of the LMC’s disc due to the combined influence of the SMC’s most recent fly-by and the tidal field of the Milky Way.

Key words: Milky Way – galaxies: dwarf – galaxies: structure – Local Group – stars

1 INTRODUCTION

Stellar discs are fragile and even a quick, low mass-ratio encounter with a neighboring galaxy can cause plenty of damage. The blockbuster by [Toomre & Toomre \(1972\)](#) provides a gallery of salient moments of such interactions as well as a comprehensive analysis of plausible outcomes. Let us provide a digest of their findings as to the formation of arms and bridges between companion galaxies. First, [Toomre & Toomre \(1972\)](#) point out that the damage is inflicted via tidal forces, which are roughly symmetric with respect to the disc’s host. Thus, a single passage will always produce two arms (whose relative strengths depend on the perturber’s orbit) on opposite sides of the disc. No slow interaction is needed, relatively fast (parabolic) orbits will also lead to arm formation. Naturally, smaller perturbers pull out tidier, i.e. more coherent arms as the fly-by of a massive neighbor causes a messier debris splatter. However, smaller perturbers take more time to pull out long arms and have to come closer to the disc compared to the massive ones. [Toomre & Toomre \(1972\)](#) highlight repeatedly how narrow the tidally-induced arms are, but take care to point out that this thinness is quite often the result of the perspective, in fact most arms are “ribbons”, not “strings”. While arm production can be thought of as a resonance phenomenon (see also [D’Onghia et al. 2010](#)), even highly inclined encounters produce dramatic arms. In the latter cases, arms usually twist considerably in 3D, and while appearing face-on for some viewing angles are clearly pulled out of the disc plane.

While the study of [Toomre & Toomre \(1972\)](#) is motivated by such iconic images as that of e.g. M51, one can find several *very local* examples of low mass-ratio galaxy conflicts with dramatic consequences. Most notably, as described in [Laporte et al.](#)

(2017) and [Laporte et al. \(2018\)](#), the Sgr dwarf - itself barely a twentieth of the Milky Way’s mass - has likely wrought plenty of havoc in the Galaxy’s disc. The dwarf is now held responsible for inducing a large-scale spiral structure in the Galaxy (see e.g. [Purcell et al. 2011](#)), creating a warp in the gaseous disc (see e.g. [Gibbons et al. 2017](#)) and sending large-amplitude waves through the stellar disc (e.g. [Widrow et al. 2012](#); [Schönrich & Dehnen 2017](#); [Xu et al. 2015](#)). Most interesting are the long thin streams of stars likely pulled out of the Galactic disc (see [Grillmair 2006, 2011](#); [de Boer et al. 2018](#); [Deason et al. 2018](#)) that do look remarkably similar to the tidal arms described in [Toomre & Toomre \(1972\)](#) and that can now be used for a variety of chemo-dynamical studies of both the Milky Way and the Sgr (see [Laporte et al. 2018](#)).

It so happened that the most striking example of a nearby binary interaction was only just being discovered at the time of writing of [Toomre & Toomre \(1972\)](#) and hence could not be included in their analysis. [Wannier & Wrixon \(1972\)](#) and [van Kuilenburg \(1972\)](#) detected long streams of HI in the Southern sky, and some two years later these were shown to connect to the Magellanic Clouds by [Mathewson et al. \(1974\)](#). The Magellanic Stream (as it is known today) has since been mapped across the sky (see e.g. [Putman et al. 2003](#); [Nidever et al. 2008, 2010](#)) and is today unambiguously demonstrated to have originated in the interaction between the Large and the Small Clouds ([Besla et al. 2007, 2010](#); [Diaz & Bekki 2011, 2012](#)). While the stellar counterpart to the MS is yet to be discovered, the last two years have seen a marked increase in the number of papers reporting detections of low surface-brightness stellar substructure in the vicinity of the Clouds (see e.g. [Mackey et al. 2016](#); [Belokurov & Koposov 2016](#); [Belokurov et al. 2017](#); [Deason et al. 2017](#); [Pieres et al. 2017](#); [Mackey et al. 2018](#); [Nidever et al. 2018](#)). In particular, [Mackey et al. \(2016\)](#) and [Mackey et al. \(2018\)](#) concentrate on the perturbations in and around the LMC’s stellar disc.

* E-mail: vasily@ast.cam.ac.uk

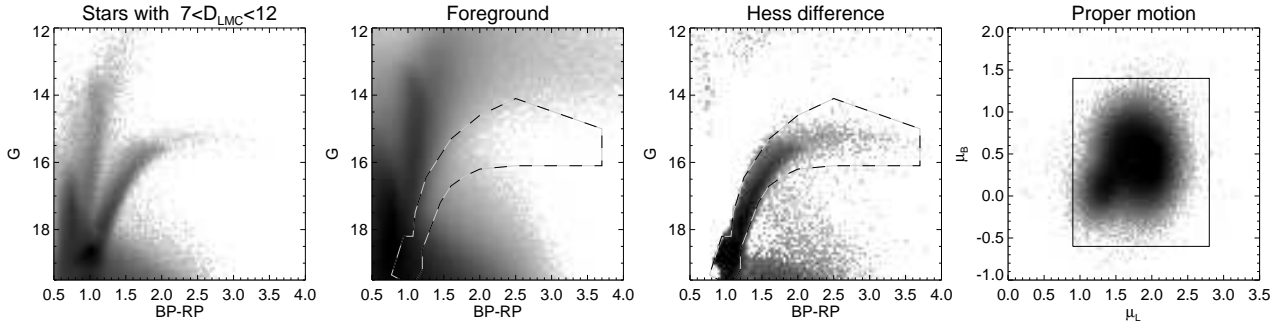


Figure 1. The Magellanic Clouds in Gaia DR2. Only stars with parallax $\varpi < 0.2$ are used. *Left:* Logarithm of the density of the outer LMC stars in the space of G vs $G_{BP} - G_{RP}$ (all de-reddened). *Middle Left:* Logarithm of the density of stars in the Galactic foreground near the Clouds. *Middle Right:* The difference of the CMD densities shown in the first two panels. Apart from some minor contamination at faint G and red $G_{BP} - G_{RP}$, the strongest over-density is that corresponding to the LMC’s red giant branch. The black-white dashed line shows the CMD mask used to select the likely LMC (and SMC) giants. *Right:* Logarithm of stellar density in proper motion space. In addition to the CMD selection shown in the middle panels, we select stars within 15° (10°) of the LMC’s (SMC’s) center and with $G_{BP} - G_{RP} > 1.3$. Black lines outline the proper motion selection box used to improve purity of the tracer population.

They uncover a wealth of sub-structure, some of which (such as the long stream-like feature in the North of the LMC) they tentatively attribute to the tidal influence of the MW (see Mackey et al. 2016). They also detect prominent stellar debris over-densities in the Southern parts of the LMC and put forward two formation scenarios: one to do with the disruption of the LMC’s disc and one linked to the episodic stripping of the SMC (see also Besla et al. 2016, who argued for the importance of repeated interactions with the SMC).

In this Letter, we use a combination of Gaia’s (Data Release 2, or GDR2) photometry and astrometry to produce an uninterrupted panorama of the Magellanic Clouds. We focus on the density fluctuations between 10 and 30 degrees away from the LMC’s centre. While our maps do not attain the same level of detail achievable using deep imaging with instruments such as DECam, they help to fill in the gaps in the Magellanic puzzle. Moreover, the Gaia’s astrometry has the unprecedented power to remove the bulk of the intervening Milky Way’s disc population and thus extend the study of the Clouds to the regions not accessible even to the deepest imaging surveys. Specifically, we demonstrate that two long and narrow tidal arms exist in the Northern and Southern outskirts of the LMC’s disc, most likely produced as a result of the combined effect of the Milky Way tides and the interaction with the SMC during its most recent passage near the Large Cloud.

2 GAIA DR2 VIEW OF THE MAGELLANIC CLOUDS

In what follows we use the photometry and astrometry provided as part of the Data Release 2 (Gaia Collaboration et al. 2018a) of the Gaia mission (Gaia Collaboration et al. 2016). We correct the G , G_{BP} and G_{RP} magnitudes for the effects of extinction using the first two terms in the Equation 1 of Gaia Collaboration et al. (2018b) and the dust maps of Schlegel et al. (1998). Additionally, we remove the foreground dwarf stars from our sample by culling all objects with parallax $\varpi > 0.2$ and exclude stars with Galactic latitudes $|b| < 5^\circ$. We note that this is not the first attempt to use GDR2 to study the LMC (and the SMC): the kinematic view of the inner portions of each Cloud can be found in Gaia Collaboration et al. (2018c), while Vasiliev (2018) presents the first results of dynamical modelling of the inner LMC.

Figure 1 shows the behavior of stars with $\varpi < 0.2$ in the vicinity of the Clouds in the color-magnitude and proper motion

spaces. More precisely, the left panel displays the density of stars within 12 degrees of the LMC’s center in G vs $G_{BP} - G_{RP}$ plane (Hess diagram). Here we assumed that the center of the dwarf is located at $\alpha, \delta = 80.89375^\circ, -69.7561^\circ$. The CMD signal of the LMC can be compared to that of the Galactic foreground shown in the second panel of the Figure. We also give the difference of the two in the third panel. In this Hess difference plot, the LMC’s Red Giant Branch (RGB) and the Red Clump (RC) are easily discernible (their envelope is traced by black-and-white dashed line). Note that the tip of the RGB runs horizontally (i.e. at constant G) for colors redder than $G_{BP} - G_{RP} \simeq 2$. While the RC is the most densely populated CMD feature, it is also the one that suffers the highest Galactic foreground contamination, especially at $G_{BP} - G_{RP} < 0.9$ and $G > 19$. Therefore, to select the likely Magellanic stars we choose objects with $\varpi < 0.2$ that fall within the CMD mask (broad enough to accommodate the heliocentric distance change across the Magellanic system) shown in panels 2 and 3 of Figure 1 and have $G_{BP} - G_{RP} > 0.9$ and $G < 19$. Finally, to further improve the purity of our selection we apply proper motion cuts chosen to delineate the motion of genuine LMC and SMC stars as shown in the fourth (rightmost) panel of the Figure. Here, stars within 15° of the LMC and 7° of the SMC are shown in μ_L, μ_B proper motion space aligned with the gaseous MS (see Nidever et al. 2008, for the definition of the L_{MS}, B_{MS} coordinate system). Note that to clarify the over-densities corresponding to the Clouds, for this panel only, we additionally limit the stars to those with $G_{BP} - G_{RP} > 1.3$.

The density of the likely Magellanic RGB candidate stars selected using a combination of parallax, $|b|$, CMD and proper motion cuts described above is shown in Figure 2. The same density map is displayed twice, in the middle and right panels of the Figure, albeit with different saturation levels to help study features across a wide range of surface brightness values. Note that even at astonishingly low Galactic latitudes, $|b| < 10^\circ$, very little disc contamination is visible thanks to the power of Gaia’s astrometry. Comparing the stellar density patterns in panels 2 and 3 with the dust distribution shown in panel 1, we conclude that, the only noticeable correlation between the two maps can be seen in the very cores of each Cloud, where the star counts are depleted by high values of extinction. Figure 2 reveals an intricate and spatially extended system of narrow stream-like structures emanating from the LMC’s disc. A large portion of the Northern arm was already discussed in Mackey et al. (2016), where it was traced out to $\sim 20^\circ$ away from

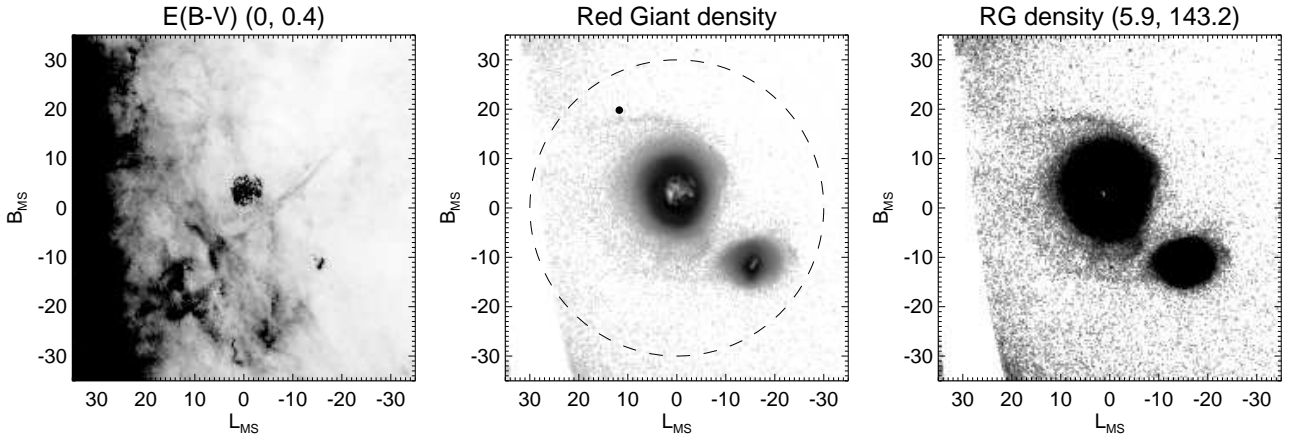


Figure 2. *Left:* Map of the distribution of the total dust extinction centered on the LMC as measured by [Schlegel et al. \(1998\)](#) *Middle:* Density of the candidate RGB stars selected using cuts illustrated in Figure 1 and described in the main text. *Right:* Same as Middle but saturated at lower density levels. Number of stars per square degree corresponding to the white (low density) and black (high density) is given in the title.

the LMC’s center. Here we show that this structure continues to higher L_{MS} for (at least) some 5° to 10° . In the Southern regions of the LMC, a more complicated web of sub-structures can be seen. There are two “claw”-like over-densities, identified as “Substructure 1” and “Substructure 2” in [Mackey et al. \(2018\)](#). Curiously, in the maps presented here, “Substructure 2” appears to be curving clockwise, continuing as far as $(L_{MS}, B_{MS}) = (10^\circ, -5^\circ)$. One of the most striking new features is a thin stellar stream which appears to be connecting to the SMC at around $L_{MS} \sim -8^\circ$. This narrow tail, one of the longest structures discussed here, wraps around the Southern edge of the LMC’s disc, tracing an arc of $\sim 90^\circ$ in clockwise direction. As gleaned from Figure 2, the LMC appears to have two long arms, one in the North and, its counter-part in the South.

To clarify the origin of the stellar over-densities described above, Figure 3 gives the proper motions of the selected LMC’s candidate RGB stars. Note that these proper motions have been corrected for the Solar reflex assuming a constant heliocentric distance of 49.9 kpc. The pattern of the median proper motion values (left column of the Figure) across the inner 10° (smaller dashed circle) is dominated by the gradient associated with the Cloud’s rotation (see also [Vasiliev 2018](#)). Note, however, that the stellar motions preserve coherence well outside the central LMC. More fascinating still, all of the narrow arm-like features at distances beyond $\sim 15^\circ$ also display coherent systematic motions. Overall, the kinematics of the Northern and Southern arms resembles that of the outer LMC’s disc but off-set in orbital phase. Note that the bulk of the Southern sub-structure shares the proper motion of the LMC. This is especially evident in the lower left panel, where the stellar streams have colors from green to red, similar the LMC’s disc, while the SMC is dark blue. While not the main focus of this Letter, it is worth commenting briefly on the proper motion pattern of the SMC. According to Figure 3, the SMC’s systemic motion is in the direction away from the LMC, i.e. towards negative L_{MS} and negative B_{MS} , consistent with previous measurements (see e.g. [Kallivayalil et al. 2013](#)). Also visible are clear proper motion gradients, whose direction is roughly aligned with the line connecting the centers of the two Clouds. While this gradient could be modelled as the rotation signal (see e.g. [Gaia Collaboration et al. 2018c](#)), we suggest it could instead be interpreted as the evidence for the strong tidal stretching of the SMC by the LMC (see also [Zivick et al. 2018](#)).

The right column of the Figure presents dispersions around the median values of proper motion components μ_L and μ_B for each

pixel of L_{MS} and B_{MS} . Strong perturbations of the inner LMC’s disc have recently been reported in the literature (see [Choi et al. 2018](#)), but here, we offer a much more complete map of kinematically cold (blue) and hot (red) regions across the entire Cloud. The regions of elevated dispersion are clearly different for the longitudinal and latitudinal proper motion components. For μ_L , the hottest region is on the rim of the LMC’s disc facing the SMC and in between the Clouds, where one naturally expects a mixture of stars from both dwarfs. In μ_B , there are two extended regions with high proper motion dispersion, one in the North and one in the South, located radially inward from the locations of each arm. The arms themselves are distinctly cold as judged by their dark blue color.

3 SIMULATIONS, CAVEATS AND CONCLUSIONS

In order to investigate how the Milky Way and SMC affect the LMC’s disc and whether they can induce the spiral features shown in Figure 2, we have run a series of simulations in the spirit of [Toomre & Toomre \(1972\)](#). In particular, we simulate the disc of the LMC as a series of particles in concentric rings which are initially on circular orbits and evolve the system in the combined presence of the Milky Way and the SMC. We model the LMC as a Hernquist profile ([Hernquist 1990](#)) which satisfies the rotation curve measurement at a radius of 8.7 kpc from [van der Marel & Kallivayalil \(2014\)](#) (for each LMC mass, the scale radius is fixed by this constraint). The initial orientation and rotation sense of the LMC are chosen to match the observations from [van der Marel & Kallivayalil \(2014\)](#). The SMC is also modelled as a Hernquist profile which satisfies the rotation curve measurement at a radius of 3 kpc from [Stanimirović et al. \(2004\)](#). The Milky Way is modelled as the 3-component potential, `MWPotential2014`, from [Bovy \(2015\)](#). Starting from their present day positions, the LMC and SMC are rewound for 1 Gyr (in the combined presence of each other and the Milky Way), at which point particles are placed on circular orbits around the LMC. For each simulation, we place 5000 particles on 50 separate concentric circles (with radii evenly spaced between 1 and 20 kpc). The simulation is then evolved to the present. For the LMC’s present day position and velocity, we use a distance of 49.97 ± 1.126 kpc ([Pietrzyński et al. 2013](#)), a radial velocity of -262.2 ± 3.4 km/s ([van der Marel et al. 2002](#)), and proper motions of $(\mu_\alpha \cos \delta, \mu_\delta) = (1.91 \pm 0.02, 0.229 \pm 0.047)$ mas/yr

(Kallivayalil et al. 2013). For the SMC’s present day position and velocity, we use a distance of 62.1 ± 1.9 kpc (Graczyk et al. 2014), a radial velocity of 145.6 ± 0.6 km/s (Harris & Zaritsky 2006), and a proper motions of $(\mu_\alpha \cos \delta, \mu_\delta) = (0.772 \pm 0.063, -1.117 \pm 0.061)$ mas/yr (Kallivayalil et al. 2013). For each choice of the LMC and SMC masses and scale radii, we sample their present day position and velocity and simulate 100 realizations to explore the variety of outcomes.

In Figure 4 we isolate the effect of the Milky Way (left-most column) and the SMC (middle two columns) on the LMC. The two rows show two different realizations of the LMC and SMC’s present day position and velocity. The top row shows an LMC with a closer encounter with the SMC ($r_{\text{peri}} \sim 10$ kpc), while the bottom row shows a more distant encounter ($r_{\text{peri}} \sim 15$ kpc). The tidal field of the Milky Way is primarily responsible for bending the Northern half of the LMC, similar to what was found in N -body simulations in Mackey et al. (2016), and creates a spiral arm feature similar in position and orientation to what it seen in the data. The SMC can create one or two spiral arms, depending on how strong of an interaction it has with the LMC during its most recent pericenter. While this is in seeming contradiction to the results of Toomre & Toomre (1972), we stress that we are observing the LMC disc only ~ 150 Myr after its most recent passage with the SMC and that it takes time for the spiral features to form. If the LMC was simulated for longer, the second spiral would form in the lower panel of Figure 4. Interestingly, we find that the SMC creates a strong spiral arm in the South which matches the observed spiral arm. We found that changing the SMC mass from $5 \times 10^9 M_\odot$ to $10^{10} M_\odot$ resulted in only a modest change in the spiral features. Our simulations do not contain the “claw”-like features visible in the data in the Southern parts of the LMC. We conjecture that these density features are remnants of much earlier interactions between the two Clouds. The fourth column of the figure shows the combined effect of the Milky Way and the SMC. This shows that their combined effect is needed to create the two spirals observed in the LMC. It also shows that a close encounter with the SMC can truncate the Western portion of the LMC’s disc (top, second from the right panel) similar to what it seen in the data. Taken together, this shows that morphology of the LMC’s disc and the associated spiral structure can be used to reveal its rich dynamical history.

In a similar vein, we also explore the effect of the LMC’s mass on its morphology in Figure 4. While the first four columns show a $2 \times 10^{10} M_\odot$ LMC, the final column shows a $2 \times 10^{11} M_\odot$ LMC. Note that the final column should be compared with the fourth column since these have the same setup. As the LMC mass is increased, we find that the LMC is deformed less by the Milky Way. This is because the increased LMC mass results in a larger tidal radius and hence a larger region where the effect of the Milky Way is negligible. Interestingly, only the lowest mass LMC we consider ($2 \times 10^{10} M_\odot$) can match the tightly wound spiral seen in the North (see Fig. 2). Since this mass is only slightly higher than the mass constraint within 8.7 kpc from van der Marel & Kallivayalil (2014), this could suggest that the LMC has already been significantly stripped. However, we stress that these simulations are only meant to be the first step in showing that the morphology (including spirals) of the LMC’s disc can provide useful constraints on the properties of the LMC, SMC, and on the tidal effect of the Milky Way. With this aim in mind, the rich proper motions in Figure 3 will be useful in future modelling efforts.

In summary, we have used the exquisite data from *Gaia* DR2 to unveil a global view of the perturbations to the LMC’s disc. In particular, there are two clear spiral features, as well as some messy

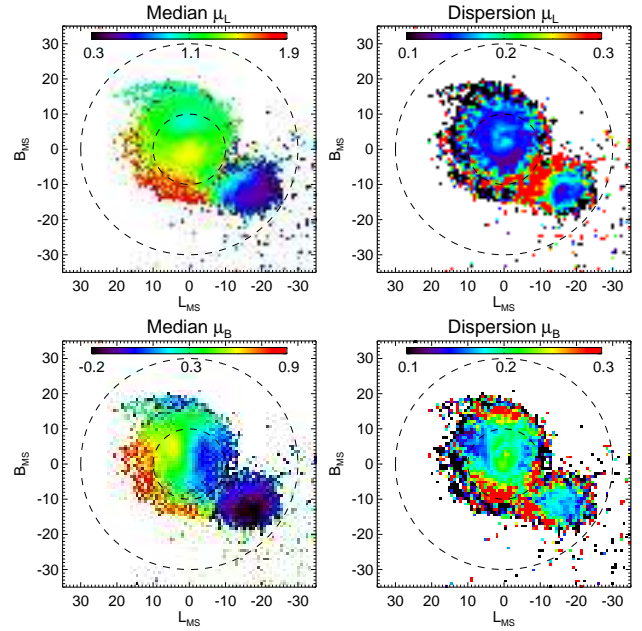


Figure 3. Kinematics of the selected RG stars. *Left Column:* Median values of μ_L (top) and μ_B (bottom) PM components in each pixel of $L_{\text{MS}}, B_{\text{MS}}$. *Right Column:* PM dispersion (around the median) maps corresponding to the median motion maps shown in the left column.

substructure to the South of the LMC (see Fig. 2). While some of this structure was seen before (e.g. Mackey et al. 2016, 2018), the uninterrupted view afforded by *Gaia* allows us to better understand how these features arose. We simulated the combined effect of the Milky Way and SMC on the LMC’s disc and found that both are important for creating the spiral features seen in the data. Namely, the Milky Way is responsible for deforming the Northern part of the LMC while the most recent passage of the SMC creates the strong spiral feature in the South. A close passage with the SMC can also truncate the Western side of the LMC’s disc. Finally, we propose to use the distant Magellanic Red Giants detected here to map out the LMC’s mass distribution at unprecedentedly large distances.

ACKNOWLEDGMENTS

We would like to thank Adrian Price-Whelan, David Hogg, Gurtian Besla, Dougal Mackey, and David Schiminovich for illuminating discussions. The research leading to these results has received funding from the European Research Council under the European Union’s Seventh Framework Programme (FP/2007-2013) / ERC Grant Agreement n. 308024. This research was started at the NYC *Gaia* DR2 Workshop at the Center for Computational Astrophysics of the Flatiron Institute in 2018 April. This work has made use of data from the European Space Agency (ESA) mission *Gaia* (<http://www.cosmos.esa.int/gaia>), processed by the *Gaia* Data Processing and Analysis Consortium (DPAC, <http://www.cosmos.esa.int/web/gaia/dpac/consortium>). Funding for the DPAC has been provided by national institutions, in particular the institutions participating in the *Gaia* Multilateral Agreement.

REFERENCES

Belokurov V., Koposov S. E., 2016, *MNRAS*, **456**, 602

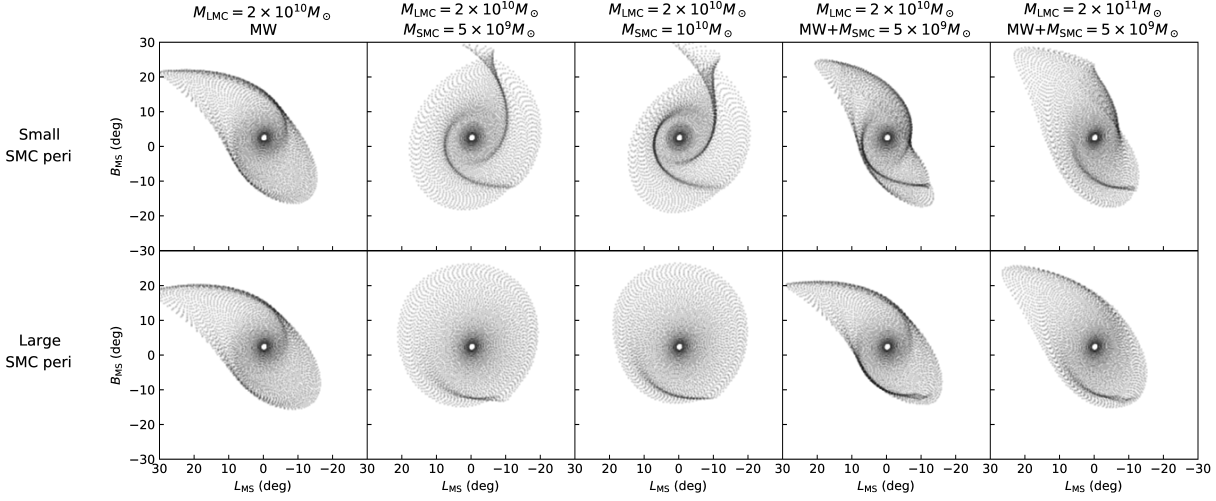


Figure 4. Map of a simulated LMC disc in the presence of the Milky Way and the SMC. Each panel shows the LMC disc in Magellanic stream coordinates. The left-most set of columns show the LMC evolved in the presence of only the Milky Way. The second (third) set of columns shows the LMC evolved in the presence of only a $5 \times 10^9 M_\odot$ ($10^{11} M_\odot$) SMC. The fourth column shows the fiducial LMC evolved in the combined presence of the Milky Way and a $5 \times 10^9 M_\odot$ SMC while the fifth column shows a $2 \times 10^{11} M_\odot$ LMC evolved in the same setup. The two rows show two different realizations of LMC and SMC from sampling their distances, radial velocities, and proper motions. The top (bottom) row shows an LMC with a closer (more distant) encounter with the SMC. These panels show that the Milky Way and SMC are responsible for different features in the LMC disc. The tidal field of the Milky Way predominantly bends the Northern part of the LMC disc, creating one of the spiral features. The influence of the SMC can create one or two spiral arms with the Southern spiral being more prominent. Together, the Milky Way and SMC create two spirals as seen in the Gaia data (i.e. Fig. 2). Finally, the rightmost column shows that increasing the LMC mass results in a smaller deflection of the LMC disc due to the Milky Way.

Belokurov V., Erkal D., Deason A. J., Koposov S. E., De Angeli F., Evans D. W., Fraternali F., Mackey D., 2017, *MNRAS*, **466**, 4711
Besla G., Kallivayalil N., Hernquist L., Robertson B., Cox T. J., van der Marel R. P., Alcock C., 2007, *ApJ*, **668**, 949
Besla G., Kallivayalil N., Hernquist L., van der Marel R. P., Cox T. J., Kereš D., 2010, *ApJ*, **721**, L97
Besla G., Martínez-Delgado D., van der Marel R. P., Beletsky Y., Seibert M., Schlafly E. F., Grebel E. K., Neyer F., 2016, *ApJ*, **825**, 20
Bovy J., 2015, *ApJS*, **216**, 29
Choi Y., et al., 2018, preprint, [p. arXiv:1805.00481](https://arxiv.org/abs/1805.00481)
D’Onghia E., Vogelsberger M., Faucher-Giguere C.-A., Hernquist L., 2010, *ApJ*, **725**, 353
Deason A. J., Belokurov V., Erkal D., Koposov S. E., Mackey D., 2017, *MNRAS*, **467**, 2636
Deason A. J., Belokurov V., Koposov S. E., 2018, *MNRAS*, **473**, 2428
Diaz J., Bekki K., 2011, *MNRAS*, **413**, 2015
Diaz J. D., Bekki K., 2012, *ApJ*, **750**, 36
Gaia Collaboration et al., 2016, *A&A*, **595**, A1
Gaia Collaboration et al., 2018c, preprint, ([arXiv:1804.09381](https://arxiv.org/abs/1804.09381))
Gaia Collaboration et al., 2018b, preprint, ([arXiv:1804.09378](https://arxiv.org/abs/1804.09378))
Gaia Collaboration Brown A. G. A., Vallenari A., Prusti T., de Bruijne J. H. J., Babusiaux C., Bailer-Jones C. A. L., 2018a, preprint, ([arXiv:1804.09365](https://arxiv.org/abs/1804.09365))
Gibbons S. L. J., Belokurov V., Evans N. W., 2017, *MNRAS*, **464**, 794
Graczyk D., et al., 2014, *ApJ*, **780**, 59
Grillmair C. J., 2006, *ApJ*, **651**, L29
Grillmair C. J., 2011, *ApJ*, **738**, 98
Harris J., Zaritsky D., 2006, *AJ*, **131**, 2514
Hernquist L., 1990, *ApJ*, **356**, 359
Kallivayalil N., van der Marel R. P., Besla G., Anderson J., Alcock C., 2013, *ApJ*, **764**, 161
Laporte C. F. P., Johnston K. V., Gómez F. A., Garavito-Camargo N., Besla G., 2017, preprint, ([arXiv:1710.02538](https://arxiv.org/abs/1710.02538))
Laporte C. F. P., Johnston K. V., Tzanidakis A., 2018, preprint, ([arXiv:1803.11198](https://arxiv.org/abs/1803.11198))
Mackey A. D., Koposov S. E., Erkal D., Belokurov V., Da Costa G. S.,

Gómez F. A., 2016, *MNRAS*, **459**, 239
Mackey D., Koposov S., Da Costa G., Belokurov V., Erkal D., Kuzma P., 2018, *ApJ*, **858**, L21
Majewski S. R., Ostheimer J. C., Patterson R. J., Kunkel W. E., Johnston K. V., Geisler D., 2000, *AJ*, **119**, 760
Mathewson D. S., Cleary M. N., Murray J. D., 1974, *ApJ*, **190**, 291
McMonigal B., et al., 2014, *MNRAS*, **444**, 3139
Nidever D. L., Majewski S. R., Butler Burton W., 2008, *ApJ*, **679**, 432
Nidever D. L., Majewski S. R., Butler Burton W., Nigra L., 2010, *ApJ*, **723**, 1618
Nidever D. L., et al., 2018, preprint, ([arXiv:1805.02671](https://arxiv.org/abs/1805.02671))
Pieres A., et al., 2017, *MNRAS*, **468**, 1349
Pietrzyński G., et al., 2013, *Nature*, **495**, 76
Purcell C. W., Bullock J. S., Tollerud E. J., Rocha M., Chakrabarti S., 2011, *Nature*, **477**, 301
Putman M. E., Staveley-Smith L., Freeman K. C., Gibson B. K., Barnes D. G., 2003, *ApJ*, **586**, 170
Schlegel D. J., Finkbeiner D. P., Davis M., 1998, *ApJ*, **500**, 525
Schönrich R., Dehnen W., 2017, preprint, ([arXiv:1712.06616](https://arxiv.org/abs/1712.06616))
Stanimirović S., Staveley-Smith L., Jones P. A., 2004, *ApJ*, **604**, 176
Toomre A., Toomre J., 1972, *ApJ*, **178**, 623
Vasiliev E., 2018, preprint, ([arXiv:1805.08157](https://arxiv.org/abs/1805.08157))
Wannier P., Wrixon G. T., 1972, *ApJ*, **173**, L119
Widrow L. M., Gardner S., Yanny B., Dodelson S., Chen H.-Y., 2012, *ApJ*, **750**, L41
Xu Y., Newberg H. J., Carlin J. L., Liu C., Deng L., Li J., Schönrich R., Yanny B., 2015, *ApJ*, **801**, 105
Zivick P., et al., 2018, preprint, ([arXiv:1804.04110](https://arxiv.org/abs/1804.04110))
de Boer T. J. L., Belokurov V., Koposov S. E., 2018, *MNRAS*, **473**, 647
van Kuilenburg J., 1972, *A&A*, **16**, 276
van der Marel R. P., Kallivayalil N., 2014, *ApJ*, **781**, 121
van der Marel R. P., Alves D. R., Hardy E., Suntzeff N. B., 2002, *AJ*, **124**, 2639